This is the accepted manuscript made available via CHORUS. The article has been published as:

# Tensile Instability in a Thick Elastic Body

Johannes T. B. Overvelde, David M. J. Dykstra, Rijk de Rooij, James Weaver, and Katia Bertoldi

Phys. Rev. Lett. **117**, 094301 — Published 24 August 2016

DOI: 10.1103/PhysRevLett.117.094301

# Tensile Instability in a Thick Elastic Body

Johannes T. B. Overvelde,[1,2] David M. J. Dykstra,[1] Rijk de Rooij,[1] James Weaver,[3] and Katia Bertoldi[1,4,*]

[1] *John A. Paulson School of Engineering and Applied Sciences, Harvard University, Cambridge, MA 02138*
[2] *FOM Institute AMOLF, Science Park 104, 1098 XG Amsterdam, The Netherlands*
[3] *Wyss Institute for Biologically Inspired Engineering, Harvard University, Cambridge, MA 02138*
[4] *Kavli Institute, Harvard University, Cambridge, MA 02138*

A range of instabilities can occur in soft bodies that undergo large deformation. While most of them arise under compressive forces, it has previously been shown analytically that a tensile instability can occur in an elastic block subjected to equitriaxial tension. Guided by this result, we conducted centimeter-scale experiments on thick elastomeric samples under generalized plane strain conditions and observed for the first time this elastic tensile instability. We found that equibiaxial stretching leads to the formation of a wavy pattern, as regions of the sample alternatively flatten and extend in the out-of-plane direction. Our work uncovers a new type of instability that can be triggered in elastic bodies, enlarging the design space for smart structures that harness instabilities to enhance their functionality.

A variety of instabilities can be triggered when elastic structures are subjected to mechanical loadings [1, 2]. While such instabilities have traditionally been considered as the onset of failure, a new trend is emerging in which the dramatic geometric changes induced by them are harnessed to enable new functionalities [3–6]. For example, buckling of thin beams and shells has been instrumental in the design of stretchable electronics [7, 8], complex 3D architectures [9, 10], materials with negative Poisson's ratio [11–13], and tunable acoustic metamaterials [14, 15]. Moreover, changes in surface curvature due to wrinkling and creases have enabled the control of surface chemistry [16], wettability [17], adhesion [18, 19], and drag [20].

While most elastic instabilities are the result of compressive forces, elastic bodies may also become unstable under tensile loading. For example, a wrinkling instability can be triggered in a thin elastic sheet under uniaxial extension [21–23], and a meniscus instability can occur when a thin layer of elastic material is confined and pulled in the out-of-plane direction resulting in a periodic array of fingers at its edges [24, 25]. Moreover, it is well-known that a cavity can undergo a sudden expansion upon reaching a critical internal pressure. This instability is not only observed in the case of thin membranes [26, 27], but also persists in thick solid bodies where it is often referred to as cavitation [28]. Since cavitation is the only tensile instability that has been found in thick elastic bodies, a natural question to ask is whether other elastic tensile instabilities can occur in such systems.

About half a century ago, it was shown analytically that a tension instability can be triggered in a block of incompressible elastic material subjected to equitriaxial tension (Fig. 1(a)) [29–33]. More specifically, it has been demonstrated that when a cube with edges of length $L$ and made from an incompressible Neo-Hookean material with initial shear modulus $\mu$, is subjected to uniform tractions resulting in six tensile normal forces of magnitude $F$, two possible equilibrium solutions exist (Supplemen-

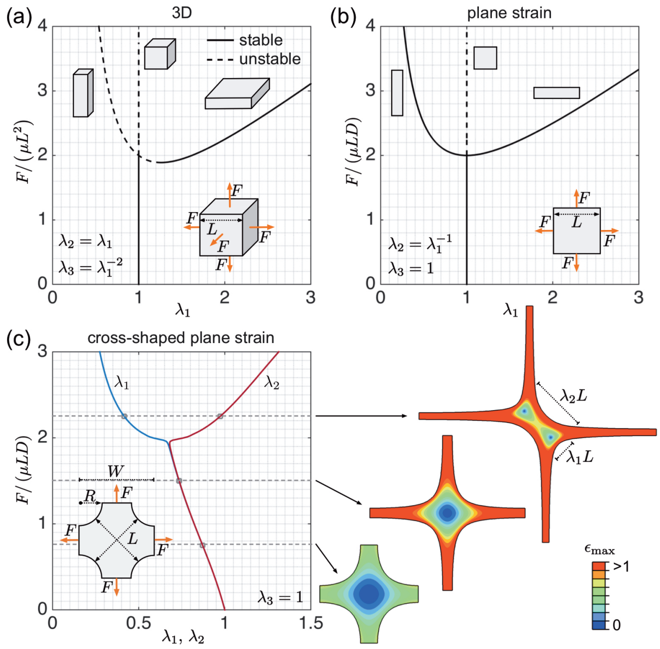


FIG. 1: Force-stretch bifurcation diagram for (a) a cube subjected to triaxial tension, (b) a square under plane strain conditions subjected to biaxial tension and (c) a biaxially stretched cross-shaped sample under plane strain conditions. The solid and dashed lines represent stable and unstable load paths, respectively. The contours show the maximum in-plane principal strain. Note that (a) and (b) were obtained analytically, while (c) was obtained using finite element analysis.

tal Material: *Analytical exploration* [34])

$$\lambda_1 = \lambda_2 = \lambda_3 = 1, \tag{1}$$

and

$$\frac{F}{\mu L^2} = \lambda_1 + \frac{1}{\lambda_1^2}, \quad \lambda_2 = \lambda_1, \quad \lambda_3 = \lambda_1^{-2}, \tag{2}$$

$\lambda_i$ being the principle stretches. As a result, when the applied force $F$ is gradually increased, the block maintains its undeformed configuration ($\lambda_i = 1$) until $F = 2\mu L^2$. At this point, the solution bifurcates, the initial branch (Eq. (1)) becomes unstable, and the cube snaps to the second branch (Eq. (2)) and therefore suddenly flattens. It should be noted that this instability has only been demonstrated analytically and has not been triggered experimentally. In this Letter, guided by both analytical and finite element models, we report the first experimental observation of this instability in a thick elastomeric sample that is stretched equibiaxially under generalized plane strain conditions.

*Designing an experiment to realize the tension instability.* Although it is possible to analytically obtain the triaxial tensile instability for a cube under triaxial tension, it is challenging to realize the same conditions in experiments. First, the instability requires the application of six equal and orthogonal forces to a block of material. Second, the forces need to be evenly spread across the whole surface, and third, the boundary conditions have to adapt to the large deformation after the instability has occured.

In an effort to simplify the boundary conditions, we start by considering an incompressible elastomeric block under plane strain conditions (i.e. $\lambda_3 = 1$ and $\lambda_2 = \lambda_1^{-1}$) subjected to four in-plane tensile forces of magnitude $F$ as indicated in Fig. 1(b). When assuming a Neo-Hookean material, the potential energy of the system, $\Pi$, is given by

$$\Pi = \frac{\mu L^2 D}{2}\left(\lambda_1^2 + \frac{1}{\lambda_1^2} - 2\right) - FL\left(\lambda_1 + \frac{1}{\lambda_1} - 2\right), \quad (3)$$

in which $D$ is the out-of-plane thickness of the sample. The equilibrium solutions are then found by minimizing $\Pi$ (i.e. $\partial\Pi/\partial\lambda_1 = 0$), yielding

$$\lambda_1 = \lambda_2 = \lambda_3 = 1, \quad (4)$$

and

$$\frac{F}{\mu L D} = \lambda_1 + \frac{1}{\lambda_1}, \quad \lambda_2 = \lambda_1^{-1}, \quad \lambda_3 = 1, \quad (5)$$

which are stable only if

$$\frac{\partial^2 \Pi}{\partial \lambda^2} = \mu L^2 D\left(1 + \frac{3}{\lambda_1^4}\right) - FL\left(\frac{2}{\lambda_1^3}\right) > 0. \quad (6)$$

Interestingly, the solutions defined by Eqs. (4)-(5) are similar to those found for the triaxial case (Eqs. (1)-(2)) and still show a bifurcation point at $F = 2\mu LD$. Differently, for the plane strain case, no snap-through instability is observed since the force monotonically increases, as indicated in Fig. 1(b). Note that during loading the out-of-plane tensile stress that builds up in the material due to the plane strain conditions plays an important role, since no instability occurs if we assume plane stress conditions (Supplemental Material: *Analytical exploration* [34]).

Next, to apply uniformly distributed traction forces to the edges of the square, we consider a cross-shaped specimen, as typically done for biaxial experiments [35, 36]. More specifically, we consider a square of edges $W$ with circles of radius $R = 0.31W$ cut from the corners. When assuming plane strain conditions, and applying an outward displacement to the straight boundaries of the sample, we expect its center to undergo a triaxial state of stress. To compare the response of the cross-shaped sample with our analytical predictions for a square (Fig. 1(b)), we monitor the evolution of the two diagonals with initial length $L = \sqrt{2}W - 2R$ located at the center of the sample as shown in Fig. 1(c), and introduce the stretches $\lambda_1$ and $\lambda_2$ to define their deformation.

Next, to determine the response of the cross-shaped sample upon loading, we performed 2D implicit finite element analysis under plane strain conditions using Abaqus (Dassault Systèmes). We captured the material response using a nearly incompressible Neo-Hookean model characterized by a ratio between the bulk modulus, $K$, and shear modulus, $\mu$, of $K/\mu = 20$ [37]. The four straight edges of the samples were loaded by a force $F$ in their normal direction, while allowing movement in the orthogonal direction. Moreover, to break the symmetry of the structure, we introduced a small imperfection by increasing the radius of two diagonally placed holes by 0.2%.

The results of our simulations are shown in Fig. 1(c), where we report the evolution of $\lambda_1$ and $\lambda_2$ as a function of the normalized force $F/(\mu LD)$. We find that an instability is triggered at $F/(\mu LD) \approx 2$, resulting in a sudden flattening of the central part of the sample similar to that predicted by the analytical model. However, different from the analytical results shown in Fig. 1(b), our results reveal that prior to the instability the central domain slightly reduces in size (i.e. $\lambda_1 = \lambda_2 \neq 1$). This discrepancy arises because the deformation in the numerical model is not homogeneous as assumed in the analytical model (see distribution of the maximum in-plane strain $\epsilon_{\max}$ in Fig. 1(c)).

*Experimental result.* Having demonstrated numerically that an elastic instability is triggered when a cross-shaped sample under plane strain conditions is subjected to biaxial tension, we fabricated a thick sample from a silicon rubber (Ecoflex 0030, Smooth-On) with a shear modulus $\mu = 0.0216$ MPa (Fig. 2(a) and Supplemental Material: *Experiments* [34]). To constrain the out-of-plane deformation we connected each side of the sample to a stiffer silicon elastomer (Elite Double 32, Zhermack) characterized by $\mu = 0.262$ MPa [38]. Moreover, to approximate the plane strain conditions assumed in our calculations, we took $D/W \gg 1$ ($D = 132$ mm and $W = 14$ mm). Finally, we placed steel tubes inside the stiffer elastomer to connect it through cables to a rigid frame that was used to stretch the sample. Fig. 2(b) shows the observed deformation at $u/W = 2.9$, $u/2$ being the displacement applied to each straight edge. Since bound-

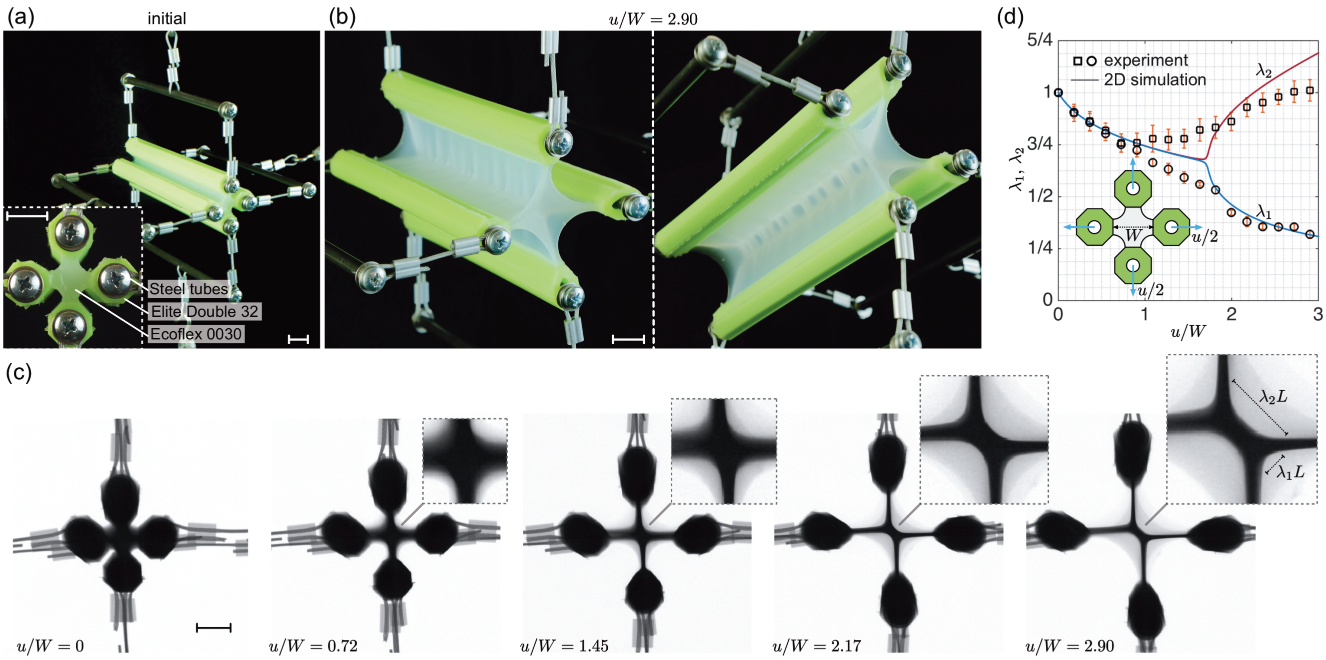


FIG. 2: (a) Experimental setup to subject our thick cross-shaped sample to biaxial tension. (b) Top and bottom views of the deformed sample at $u/W = 2.90$. (c) Cross-sectional views of the sample at $u/W = 0$, 0.72, 1.45, 2.17 and 2.90 obtained using a micro-CT X-ray imaging machine. (d) Relation between the normalized displacement, $u/W$, applied to the sample and the stretches, $\lambda_1$ and $\lambda_2$, of the diagonals located at the center of the sample. The results were obtained by manually processing the images and averaging five individual measurements (the error bars indicate the standard deviation) (scale bars 10 mm).

ary effects prevented us to clearly observe the instability (Fig. S6), we acquired x-ray transmission images at different levels of applied deformation (Fig. 2(c) and Movie 1). We then manually processed the images to obtain the stretches, $\lambda_1$ and $\lambda_2$, that define the deformation of the diagonals of the central domain, exactly as in our simulations. The results reported in Fig. 2(d) indicate that at $u/W \approx 1$ an instability is triggered that breaks the symmetry and initiates a flattening of the center of the sample. While the experimental results agree relatively well with the 2D plane strain simulations, we find that the instability is triggered for smaller deformations. This discrepancy is likely due to imperfections introduced during fabrication and loading, which tend to smoothen the sudden transition arising from the instability and result in an earlier flattening (Fig. S7).

*Wavy pattern along the depth.* From the experiments we find that the instability not only results in the flattening of the center of the sample as predicted by the plane strain simulations, but also introduces waves on the surfaces along the depth (Fig. 2(b)). To better understand the formation of this wavy pattern, we conducted 3D explicit quasi-static finite element analysis and simulated the cross-shaped sample as used in the experiments, i.e. we modeled both the two elastomeric materials and steel tubes to exactly mimic the experimental conditions [39].

As shown in Fig. 3(a) and Movie 2, our 3D simulations confirm the experimental observations. By monitoring the stretch of the diagonals defining the center region of the sample (along the depth), it becomes clear that the wavy pattern emerges the moment the sample becomes unstable at $u/W \approx 2$ (Fig. 3(b)). In fact, for $u/W \lesssim 2$ $\lambda_1$ and $\lambda_2$ are constant along the depth of the sample, while for $u/W \gtrsim 2$ they oscillate periodically. Moreover, we also find that after the instability has occurred, the sample not only deforms non-uniformly in-plane, but also in the out-of-plane direction. To highlight this point, in Fig. 3(c) we report the out-of-plane stretch, $\lambda_3$, measured along the center line of the sample at different levels of applied loading. The results indicate that for $u/W \gtrsim 2$ there is an alternation between regions experiencing out-of plane extension and compression along the depth of the sample.

Informed by the numerical results of Figs. 3(a)-(c), we next extend our analytical model and assume that the elastic block consists of two layers, $a$ and $b$, which can deform separately. We then impose generalized plane strain conditions

$$\bar{h}\lambda_{a,3} + \left(1 - \bar{h}\right)\lambda_{b,3} = 1, \tag{7}$$

where the stretches $\lambda_{a,3}$ and $\lambda_{b,3}$ are indicated in Fig. 3(d), and $\bar{h} = D_a/\left(D_a + D_b\right)$ sets the ratio between the depth of layer $a$ and $b$ in the undeformed configuration. If we further assume that the four in-plane forces applied to each layer depend on the initial size of the layer (i.e. $F_a = F\bar{h}$ and $F_b = F(1-\bar{h})$, $F$ being the total force applied to the two blocks), the potential energy takes the form (supplementary materials: *Analytical exploration*)

$$\begin{aligned}\Pi =& \frac{\bar{h}\mu L^2 D}{2}\left(\lambda_{a,1}^2 + \frac{1}{\lambda_{a,1}^2\lambda_{a,3}^2} + \lambda_{a,3}^2 - 3\right) \\ &+ \mu L^2 D \frac{1-\bar{h}}{2}\left(\lambda_{b,1}^2 + \frac{\left(1-\bar{h}\right)^2}{\lambda_{b,1}^2\left(1-\bar{h}\lambda_{a,3}\right)^2}\right. \\ &\left.+ \frac{\left(1-\bar{h}\lambda_{a,3}\right)^2}{\left(1-\bar{h}\right)^2} - 3\right) - F_a L\left(\lambda_{a,1} + \frac{1}{\lambda_{a,1}\lambda_{a,3}} - 2\right) \\ &- F_b L\left(\lambda_{b,1} + \frac{1-\bar{h}}{\lambda_{b,1}\left(1-\bar{h}\lambda_{a,3}\right)} - 2\right), \qquad (8)\end{aligned}$$

where $D = D_a + D_b$. Minimizing the energy results again in two possible solutions

$$\lambda_{a,1} = 1 \quad \text{with} \quad 0 \leq \bar{h} \leq 1, \qquad (9)$$

$$\frac{F}{\mu L D} = \lambda_{a,1} + \frac{1}{\lambda_{a,1}^2} \quad \text{with} \quad \bar{h} = \frac{\lambda_{a,1}^2 - 1}{\lambda_{a,1}^3 - 1}, \qquad (10)$$

in which $\lambda_{a,3} = \lambda_{b,1} = \lambda_{b,2} = \lambda_{a,1}$ and $\lambda_{a,2} = \lambda_{b,3} = \lambda_{a,1}^{-2}$. We find that the solutions defined by Eqs. (9)-(10) are identical to those found for a cube subjected to equitriaxial tension (Eqs. (1)-(2)), and that a bifurcation occurs at $F/(\mu L D) = 2$. For $F/(\mu L D) < 2$ the system does not deform (as illustrated in Fig. 3(e) for $F/(\mu L D) = 3/2$), while for $F/(\mu L D) > 2$ one of the layer extends and the other flattens in the out-of-plane direction (as illustrated in Fig. 3(e) for $F/(\mu L D) = 5/2$), resulting in a wavy pattern that resembles the deformation shown in Figs. 2(b) and 3(a).

*Outlook.* In this work, we experimentally showed that an instability can be triggered in a thick elastic body subjected to in-plane tensile forces and generalized plane strain conditions. While an instability was already analytically predicted in 1948 for a cube subjected to triaxial tension [29], here we extended the analysis to a configuration that can be tested experimentally, and found that the modified conditions result in a wavy pattern, as portions of the sample alternatively extend and flatten in the out-of-plane direction.

It should be noted that tensile loading conditions can also lead to cavitation in solids [28, 40]. More specifically, for an incompressible Neo-Hookean material subjected to equitriaxial tension, it can be analytically derived that cavitation initiates at a pressure of $p_{\text{cav}} = 5\mu/2$ [41]. As a result, for the elastomeric cube of Fig. 1(a) subjected to triaxial tension cavitation initiates at $F_{\text{cav}} = 5\mu L^2/2$. Although this critical value is 25% higher than that needed to flatten the cube, we expect our sample to experience such value of stress in the post-buckling regime. In fact, upon increasing the stretch applied to the sample to $u/W = 3.26$, we immediately see some cavities forming, which slowly increase in size when the applied deformation is maintained for a few hours (Movie 3).

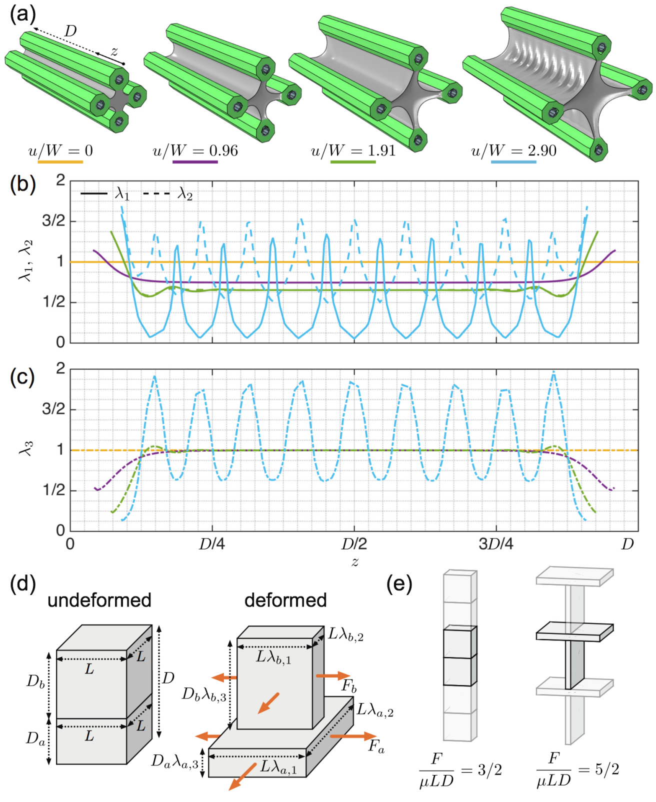


FIG. 3: (a) Numerical snapshots of the sample, (b) stretches that define the deformation of the diagonals of the central domain ($\lambda_1$ and $\lambda_2$) along the depth of the sample, and (c) out-of-plane stretch of the centerline ($\lambda_3$) along the depth of the sample, at $u/W = 0$, 0.96, 1.91, 2.90. (d) Schematic of the bilayer under generalized plane strain conditions used in our analytical model. (e) Deformed states of the analytical model at $F/(\mu L D) = 3/2$ and 5/2 for $D = 2L$.

Finally, the cross-shaped samples used in our experiments can be used to build a mechanical metamaterial by arranging them on a square lattice as shown in Fig. 4. By stretching the metamaterial biaxially (under plane strain conditions), an instability is triggered at $u/W \approx 2$ resulting in a checkerboard pattern of pores with two different sizes as indicated by the evolution of the characteristic pore sizes $l_1$ and $l_2$ shown in Fig. 4. While the formation of this pattern has previously been observed in simulations of similar periodic porous structures [42–44], with the current work we have deciphered the underlying mechanism that leads to the instability. As such, we expect our study to open new avenues for the design of soft structures that harness instabilities for improved functionality.

*Acknowledgements* This work was supported by the Materials Research Science and Engineering Center under NSF Award No. DMR-1420570. K.B. also acknowledges support from the National Science Foundation (CMMI-1149456-CAREER). We thank Samuel Shian for his initial help with the experimental setup, and Sahab

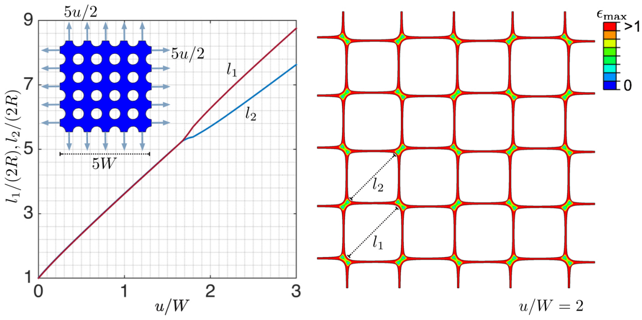


FIG. 4: Deformation of a mechanical metamaterial comprising a square array of circular pores subjected to equibiaxial tension. Similar to the case of the cross-shaped sample shown in Fig. 1(c), an instability is triggered at $u/W \approx 2$ resulting in a checkerboard pattern of pores with two different sizes. The contours represent the maximum in-plane strain $\epsilon_{\max}$.

Babaee and John Hutchinson for fruitfull discussions.

* Electronic address: `bertoldi@seas.harvard.edu`

[1] Z. Bažant and L. Cedolin, *Stability of Structures: Elastic, Inelastic, Fracture and Damage Theories* (World Scientific, 2010).
[2] Q. Wang and X. Zhao, MRS Bulletin **41** (2016).
[3] S. Singamaneni and V. V. Tsukruk, Soft Matter **6**, 5681 (2010).
[4] D. Chen, J. Yoon, D. Chandra, A. J. Crosby, and R. C. Hayward, Journal of Polymer Science Part B: Polymer Physics **52**, 1441 (2014).
[5] B. Florijn, C. Coulais, and M. van Hecke, Physical Review Letters **113** (2014).
[6] S. Cai, D. Breid, A. Crosby, Z. Suo, and J. Hutchinson, Journal of the Mechanics and Physics of Solids **59**, 1094 (2011).
[7] J. A. Rogers, T. Someya, and Y. Huang, Science **327**, 1603 (2010).
[8] Y. Wang, R. Yang, Z. Shi, L. Zhang, D. Shi, E. Wang, and G. Zhang, ACS Nano **5**, 3645 (2011).
[9] J. Kim, J. A. Hanna, M. Byun, C. D. Santangelo, and R. C. Hayward, Science **335**, 1201 (2012).
[10] S. Xu, Z. Yan, K.-I. Jang, W. Huang, H. Fu, J. Kim, Z. Wei, M. Flavin, J. McCracken, R. Wang, et al., Science **347**, 154 (2015).
[11] K. Bertoldi, P. M. Reis, S. Willshaw, and T. Mullin, Advanced Materials **22**, 361 (2010).
[12] J. T. B. Overvelde, S. Shan, and K. Bertoldi, Advanced Materials **24**, 2337 (2012).
[13] S. Babaee, J. Shim, J. C. Weaver, E. R. Chen, N. Patel, and K. Bertoldi, Advanced Materials **25**, 5044 (2013).
[14] K. Bertoldi and M. C. Boyce, Physical Review B **77**, 052105 (2008).
[15] P. Wang, F. Casadei, S. Shan, J. C. Weaver, and K. Bertoldi, Physical Review Letters **113** (2014).
[16] J. Kim, J. Yoon, and R. C. Hayward, Nature Materials **9**, 159 (2010).
[17] P.-C. Lin and S. Yang, Soft Matter **5**, 1011 (2009).
[18] P.-C. Lin, S. Vajpayee, A. Jagota, C.-Y. Hui, and S. Yang, Soft Matter **4**, 1830 (2008).
[19] E. Chan, E. Smith, R. Hayward, and A. Crosby, Advanced Materials **20**, 711 (2008).
[20] D. Terwagne, M. Brojan, and P. M. Reis, Advanced Materials **26**, 6608 (2014).
[21] E. Cerda and L. Mahadevan, Physical Review Letters **90**, 074302 (2003).
[22] B. Davidovitch, R. D. Schroll, D. Vella, M. Adda-Bedia, and E. A. Cerda, Proceedings of the National Academy of Sciences **108**, 18227 (2011).
[23] H. Vandeparre, S. Gabriele, F. Brau, C. Gay, K. K. Parker, and P. Damman, Soft Matter **6**, 5751 (2010).
[24] K. R. Shull, C. M. Flanigan, and A. J. Crosby, Physical Review Letters **84**, 3057 (2000).
[25] J. S. Biggins, B. Saintyves, Z. Wei, E. Bouchaud, and L. Mahadevan, Proceedings of the National Academy of Sciences **110**, 12545 (2013).
[26] D. R. Merritt and F. Weinhaus, American Journal of Physics **46**, 976 (1978).
[27] J. T. B. Overvelde, T. Kloek, J. J. A. D'haen, and K. Bertoldi, Proceedings of the National Academy of Sciences **112**, 10863 (2015).
[28] A. N. Gent and P. B. Lindley, Proceedings of the Royal Society of London A: Mathematical, Physical and Engineering Sciences **249**, 195 (1959).
[29] R. S. Rivlin, Philosophical Transactions of the Royal Society of London A: Mathematical, Physical and Engineering Sciences **240**, 491 (1948).
[30] R. Hill, Journal of the Mechanics and Physics of Solids **5**, 229 (1957).
[31] M. F. Beatty, International Journal of Solids and Structures **3**, 23 (1967).
[32] R. S. Rivlin, *Collected Papers of R.S. Rivlin: Volume I and II* (Springer New York, New York, NY, 1997), chap. Stability of Pure Homogeneous Deformations of an Elastic Cube under Dead Loading, pp. 398–404.
[33] J. M. Ball and D. G. Schaeffer, Mathematical Proceedings of the Cambridge Philosophical Society **94**, 315 (1983).
[34] See Supplemental Material [url], which includes Refs. [29–33, 45, 46].
[35] E. Shiratori and K. Ikegami, Journal of the Mechanics and Physics of Solids **16**, 373 (1968).
[36] Y. Lecieux and R. Bouzidi, International Journal of Solids and Structures **47**, 2459 (2010).
[37] The models were discretized using approximately $1.5 \cdot 10^4$ triangular quadratic elements (Abaqus element code CPE6). For the nearly incompressible Neo-Hookean model we chose $K/\mu = 20$, as it provides a good balance between simulation time and accuracy (Supplemental Material: *Effect of material compressibility* [34]).
[38] J. Shim, C. Perdigou, E. R. Chen, K. Bertoldi, and P. M. Reis, Proceedings of the National Academy of Sciences **109**, 5978 (2012).
[39] We modeled the Elite Double 32 and Ecoflex 0030 using a nearly incompressible Neo-Hookean material model with $K/\mu = 20$. Moreover, we assumed that the steel tubes do not deform, and used approximately $5 \cdot 10^5$ linear elements to construct the model (Abaqus element code C3D6R and C3D8R). We further assumed that the bonding region between the two elastomers is infinitesimally thin and can be neglected. Note that since we used explicit analysis we did not apply any imperfections.

[40] J. M. Ball, Philosophical Transactions of the Royal Society of London A: Mathematical, Physical and Engineering Sciences **306**, 557 (1982).

[41] A. Gent, International Journal of Non-Linear Mechanics **40**, 165 (2005).

[42] K. Bertoldi and M. C. Boyce, Physical Review B **78**, 184107 (2008).

[43] J. T. Overvelde and K. Bertoldi, Journal of the Mechanics and Physics of Solids **64**, 351 (2014).

[44] J. Michel, O. Lopez-Pamies, P. P. Castañeda, and N. Triantafyllidis, Journal of the Mechanics and Physics of Solids **55**, 900 (2007).

[45] R. Ogden, *Non-Linear Elastic Deformations* (Dover New York, 1988).

[46] M. C. Boyce and E. M. Arruda, Rubber Chemistry and Technology **73**, 504 (2000).